HHS Public Access

Author manuscript

J Cell Physiol. Author manuscript; available in PMC 2018 September 01.

Published in final edited form as:

J Cell Physiol. 2017 September ; 232(9): 2447–2460. doi:10.1002/jcp.25582.

Vertebrate Lonesome Kinase Regulated Extracellular Matrix Protein Phosphorylation, Cell Shape and Adhesion in Trabecular Meshwork Cells

Rupalatha Maddala[1], **Nikolai P. Skiba**[1], and **Ponugoti Vasantha Rao**[1,2,*]

[1]Department of Ophthalmology, Duke University School of Medicine. Durham, NC. USA. 27710

[2]Department of Pharmacology and Cancer Biology, Duke University School of Medicine. Durham, NC. USA. 27710

Abstract

Glaucoma, a leading cause of irreversible blindness is commonly associated with elevated intraocular pressure (IOP) due to impaired aqueous humor (AH) drainage through the trabecular meshwork (TM). Although dysregulated production and organization of extracellular matrix (ECM) is presumed to increase resistance to AH outflow and elevate IOP by altering TM cell contractile and adhesive properties, it is not known whether regulation of ECM protein phosphorylation via the secretory vertebrate lonesome kinase (VLK) influences TM cellular characteristics. Here we tested this possibility. Experiments carried out in this study reveal that the 32 kDa protein is a prominent VLK isoform detectable in lysates and conditioned media (CM) of human TM cells. Increased levels of VLK were observed in CM of TM cells subjected to cyclic mechanical stretch, or treated with dexamethasone, TGF-β2 and TM cells expressing constitutively active RhoA GTPase. Downregulation of VLK expression in TM cells using siRNA decreased tyrosine phosphorylation (TyrP) of ECM proteins and focal adhesions, and induced changes in cell shape in association with reduced levels of actin stress fibers and phospho-paxillin. VLK was also demonstrated to regulate TGF-β2-induced TyrP of ECM proteins. Taken together, these results suggest that VLK secretion can be regulated by external cues, intracellular signal proteins and mechanical stretch, and VLK can in turn regulate TyrP of ECM proteins secreted by TM cells and control cell shape, actin stress fibers and focal adhesions. These observations indicate a potential role for VLK in homeostasis of AH outflow and IOP, and in the pathobiology of glaucoma.

Keywords

VLK; ECM; Trabecular meshwork; Intraocular pressure; Glaucoma

*To whom correspondence should be addressed: Duke Eye Center, 2351 Erwin Road, Durham, NC. 27710. Phone: 919-681-5883; Fax: 919-684-8983; p.rao@dm.duke.edu.

Conflict of Interest Disclosure

The authors declare that they have no conflicts of interest to disclose.

Conflicts: None

Introduction

Glaucoma is a leading cause of irreversible blindness worldwide. Elevated intraocular pressure (IOP) is a dominant risk factor for primary open angle glaucoma, the most prevalent form of glaucoma (Kwon et al., 2009b; Weinreb and Khaw, 2004). Importantly, lowering of IOP is a mainstay of treatment options to delay progressive vision loss in glaucoma patients (Kwon et al., 2009b; Weinreb and Khaw, 2004). IOP is determined by the balance between the secretion of AH by the ciliary epithelium and its drainage through the conventional and non-conventional outflow pathways(Bill, 1966; Kanski et al., 2011; Weinreb and Khaw, 2004). Five different classes of currently used topical glaucoma drugs including prostaglandin analogs, beta blockers, carbonic anhydrase inhibitors, sympathomimetics and miotics, lower IOP by either decreasing AH production or increasing AH drainage (Bucolo et al., 2013). In humans, most of the AH is drained via the conventional/trabecular pathway consisting of the trabecular meshwork (TM), juxtacanalicular tissue and Schlemm's canal (Weinreb and Khaw, 2004). Blockage or increased resistance to AH outflow in the trabecular pathway is believed to be the main cause for elevated IOP in glaucoma patients (Gabelt and Kaufman, 2005; Keller et al., 2009).

Among the various molecular and cellular mechanisms thought to be involved in increased resistance to AH outflow and increase in IOP, dysregulated production, organization and stiffness of the extracellular matrix (ECM) in response to external cues including TGF-β, connective tissue growth factor and glucocorticoids, is considered to be a dominant etiological contributor (Braunger et al., 2015; Fleenor et al., 2006; Han et al., 2011; Junglas et al., 2009; Li et al., 2004; Pattabiraman et al., 2014; Raghunathan et al., 2015; Sethi et al., 2011; Tektas et al., 2010; Vranka et al., 2015; Wallace et al., 2014). While an increase in ECM constituents and ECM stiffness have been shown to influence the contractile and cell adhesive properties of TM cells and to decrease AH outflow(Gagen et al., 2014; Pattabiraman and Rao, 2010; Raghunathan et al., 2015; Zhang et al., 2008), matrix metalloproteinase (MMP)-mediated ECM degradation was found to increase AH outflow, confirming a definitive role for ECM turnover in regulation of AH outflow through the TM (Bradley et al., 1998; Gerometta et al., 2010; Keller et al., 2009). Interestingly, both ECM and MMPs are also shown to participate in regulation of AH outflow through the con-conventional or uveo-scleral pathway (Gaton et al., 2001; Weinreb and Khaw, 2004). However, the plausible role of ectokinases or secretory kinases that catalyze posttranslational modifications such as phosphorylation of ECM proteins on TM cell properties and AH outflow has not been explored.

Based on several recent studies, it is becoming increasingly evident that ECM and other extracellular proteins including the MMPs are subject to phosphorylation and dephosphorylation mediated by various secretory kinases and phosphatases (Bordoli et al., 2014; Tagliabracci et al., 2015; Yalak and Vogel, 2012). Protein phosphorylation has been studied extensively and recognized to play a fundamental role in regulation of cellular functions in both normal and disease states (Cohen, 2002; Fischer, 2010). Secretory kinase mediated phosphorylation of ECM proteins, MMPs and several other secretory proteins occurs on serine, threonine and tyrosine residues, and utilizes extracellular ATP resulting

either from cell death or through other mechanisms (Bordoli et al., 2014; Tagliabracci et al., 2013; Tagliabracci et al., 2015; Yalak and Vogel, 2012). The secretory kinases vertebrate lonesome kinase (VLK) and Fam20C which phosphorylate various secretory proteins including the ECM proteins and MMPs, are thought to be relevant in both physiological and pathological conditions (Bordoli et al., 2014; Kinoshita et al., 2009; Simpson et al., 2007; Tagliabracci et al., 2015; Yalak and Vogel, 2015). VLK, a secretory tyrosine kinase (also known as Protein Kinase Domain Containing protein, Cytoplasmic-PKDCC and sgk493) has also been shown to regulate protein transport through the Golgi and endoplasmic reticulum, and formation of stroma and differentiation of chondrocytes (Bordoli et al., 2014; Imuta et al., 2009; Kinoshita et al., 2009). Limited knowledge is available, however, regarding the regulation of VLK expression and secretion and its physiological function.

Since increased resistance to AH outflow and elevated IOP in glaucoma patients is considered to originate partly from the dysregulation of ECM, and cell death in tissues of the trabecular pathway (Alvarado et al., 1984; Braunger et al., 2015; Vranka et al., 2015), we postulated that dysregulation of ECM phosphorylation might play a role in these etiological events via altered outside-in signaling, actin cytoskeletal reorganization, integrin mediated cell adhesion and ECM material properties. To explore this possibility, we initiated a study which for the first time, evaluates the expression, secretion and distribution profile of VLK kinase, and the effects of VLK on tyrosine phosphorylation (TyrP) of the ECM-enriched protein fraction in human TM cells. The results of this study reveal that TGF-β2, dexamethasone and cyclic mechanical stretch increase the levels of VLK in conditioned media derived from cultured TM cells, and VLK-dependent tyrosine phosphorylation of ECM and ECM-associated proteins. Our data also indicate that VLK functions to maintain TM cell shape and adhesive properties, and actin stress fiber formation, and taken collectively, suggest a role for VLK in the homeostasis of AH outflow and IOP.

Materials and Methods

Cell culture

Human TM primary cells were cultured from TM tissue isolated from donor corneal rings used for corneal transplantation at the Duke Ophthalmology Clinical Service, as we described earlier (Pattabiraman and Rao, 2010). TM cells passaged between 4 to 6 times, and derived from donor specimens ranging in age from 19 to 68 years were used in the experiments. Cells were cultured at 37°C under 5% CO2 in Dulbecco's modified Eagle's medium (DMEM) containing 10% FBS (fetal bovine serum), penicillin (100 U/ml)-streptomycin (100 μg/ml) glutamine (4 mM), in Eppendorf plastic plates and six well dishes. Most of the experiments were performed using confluent cultures under 24 h serum starvation. For determining the distribution profile of VLK in TM cells, cells were plated on glass coverslips coated with 2% gelatin.

Reverse transcription-polymerase chain reaction (RT-PCR)

Total RNA extracted from human TM cells (passage 4) using the RNeasy Mini Kit (Qiagen, Valencia, CA) was quantitated using NanoDrop 2000 UV-Vis Spectrophotometer (Thermo Scientific, Wilmington, DE). Equal amounts of RNA (DNA free) were then reverse

transcribed using the Advantage RT-for-PCR kit (Clonetech, Mountain View, CA) according to manufacturer's instructions. Controls lacking reverse transcriptase were included in the RT-PCR experiments. PCR amplification was performed on the resultant reverse transcriptase-derived single stranded cDNA using sequence-specific forward and reverse oligonucleotide primer sets specific for human VLK mRNA (NCBI: NM_138370.2) ;

set1: GGTTTCTGCGCCTCCTT/GTACACGGCCTTGGTGTAG (product size-429 bp);

set2: CGTCCTCAACGTGCTCTTC/CCTGGTAGCAGTAGCCATAGA (product size-602 bp);

set3: ACGTGCTGCAGCTCTATG/GGCAGGAGGTATGTGAAGAAA (product size-430 bp);

set4: CGAGAAGCGGAACCTCTATAATG/CTGCTTGCCGTGGAGTT (product size-210 bp);

set5: AGTACCGAGTACCAGTGTATCC/GGCTCCATCCAGTCTTGAAA (product size-217 bp) and C1000 Touch Thermocycler (Bio-Rad, Hercules, CA). The PCR reactions were carried out with a denaturation step at 94°C for 5 min, primer annealing at 60 °C for 30 seconds and primer extension at 72 °C for 45 seconds. The cycle was repeated 30 times. The resulting DNA products were separated on 1.5% agarose gels and visualized by staining with gel green reagent (Invitrogen; C. No. 41005), using a Fotodyne Trans-illuminator (Fotodyne Inc., Hartland, WI). PCR product bands were excised and sequenced to confirm identity.

siRNA transfection

Small interfering RNA (siRNA) directed against human VLK/PKDCC (C. No. sc-94454) and a corresponding, scrambled control siRNA (C. No. sc-169299) were purchased from Santa Cruz Biotechnology (Dallas, TX). Human TM cells grown in plastic 6-well plates or petri- dishes were transfected using 25 pmol human VLK siRNA (containing a mixture of three sets of interfering short RNAs) or control siRNA, the Lipofectamine RNAiMax reagent (C. No. 13778-075, Invitrogen/ThermoFisher, Waltham, MA) and Opti-MEM media (C. No. 319850-70) supplemented with antibiotics per manufacturer's instructions. Briefly, 3ml opti-MEM media containing RNAiMax reagent and the respective siRNAs were added to cells grown in culture dishes and incubated for 2 h in a humidified cell culture incubator, following which 2 ml of 10% serum containing DMEM media was added slowly. After 72 h following transfection, cells were photographed using a phase contrast microscope (Zeiss AX10) to monitor for morphological changes. Media, cells and ECM protein fractions were collected from these cultures, and processed to analyze the levels of VLK and TyrP proteins using appropriate antibodies. The volume of transfection Opti-MEM media (containing RNAiMax reagent and respective siRNAs) was adjusted accordingly for cells grown on glass cover slips and transfections were performed as mentioned above.

Cyclic mechanical stretch

Primary cultures of human TM cells were plated on collagen Type 1 BioFlex culture plates with flexible silicone bottom (C. No. BF-3001C, Flexcell® International Corporation,

Burlington, NC). As the cells reached confluence, culture medium was switched to serum-free phenol free DMEM, and cells were subjected to cyclic mechanical stretch (20% stretching, one cycle per second) for 48 h, using the computer-controlled, vacuum-operated FX-3000 Flexcell Strain Unit (Flexcell, Hillsborough, NC). Control cells were cultured under similar conditions with no mechanical force applied. Conditioned media were collected from both control and stretched cells to analyze the VLK protein levels.

Adenovirus-mediated gene transfection

Replication defective recombinant adenoviral vectors encoding either GFP (Green fluorescence protein) alone or constitutively active RhoA mutant (RhoAV14) and GFP provided by Patrick Casey, Department of Pharmacology and Cancer Biology, Duke University School of Medicine, were amplified and purified as we described earlier (Zhang et al., 2008). Human TM cells grown in petri dishes were infected with the respective adenovirus at 50 MOI (multiplicity of infection) and after 24 h (when cells exhibited >80% transfection, as assessed from GFP fluorescence), serum starved for 36 h and conditioned media were collected and cell lysates prepared to quantitate the levels of VLK protein.

Immunofluorescence analyses

Tissue sections from formalin-fixed, paraffin-embedded human eye whole globes (from donors over 50 years of age) were immunostained with VLK antibody as we previously described (Pattabiraman et al., 2015). Briefly, 5-μm-thick tissue sections were deparaffinized and rehydrated using xylene, absolute ethyl alcohol and water. To unmask the antigen epitopes, heat-induced antigen retrieval was performed using 0.1 M citrate buffer pH 6.0 (Vector Laboratories, Burlingame, CA, USA) for 20 min at 100°C. The slides were then blocked for nonspecific interaction with Biocare Medical's (Concord, CA, USA) Sniper Background Reducer (C. No. BS966). The tissue sections were then incubated overnight at 4°C in a humidified chamber with rabbit polyclonal primary antibody raised against VLK (C. No. TA306903, Origene, Rockville, MD), at a final dilution of 1:200. Primary antibody dilutions were made in 1% bovine serum albumin (BSA) in Tris-buffered saline (TBS). After incubation with a primary antibody, the slides were washed with TBS and incubated with Alexa Fluor-594 goat anti-rabbit secondary antibody (Invitrogen/ThermoFisher) for 2 h at room temperature (RT) followed by Hoechst 33342 (Invitrogen/ThermoFisher) staining at 1:1000 for 10 min. Slides were then washed with TBS buffer and mounted with Vecta Mount purchased from Vector laboratories, Burlingame, CA. Immunostaining analyses were carried out in quadruplicate, and negative controls were run simultaneously and incubated overnight with 1% BSA in TBS with no primary antibody. The immunostained slides were then viewed and imaged using a Nikon Eclipse 90i confocal laser-scanning microscope (Nikon Instruments, Melville, NY, USA).

Human TM cells grown on gelatin (2%) -coated glass coverslips were washed with PBS (phosphate buffered saline) and fixed with 4% paraformaldehyde, permeabilized, blocked and immunostained for VLK, F-actin, vinculin, phospho-paxillin and phospho-tyrosine using TRITC-phalloidin (C. No. P195; Sigma-Aldrich), rabbit polyclonal anti-VLK, mouse monoclonal anti-vinculin (C. No. V9131; Sigma-Aldrich), rabbit polyclonal anti-phospho-paxillin (C. No. 2541; Cell Signaling Tech) and rabbit monoclonal anti-phospho-tyrosine (P-

Tyr-1000; C. No. 8954; Cell Signaling Tech) antibodies, respectively, as we described previously along with appropriate secondary antibodies conjugated with fluorophore (Pattabiraman and Rao, 2010). The slides were viewed and imaged using a Nikon Eclipse 90i confocal laser-scanning microscope.

Immunoblotting

TM cells subjected to various treatments and the respective controls were homogenized at 4 C in hypotonic 10 mM Tris buffer pH 7.4 containing 0.2 mM MgCl2, 5 mM N-ethylmaleimide, 2.0 mM Na3VO4, 10 mM NaF, 60 Tm phenylmethyl sulfonyl fluoride (PMSF), 0.4 mM iodoacetamide and protease and phosphatase inhibitor cocktail (one tablet /10 ml buffer), using a probe sonicator. Homogenates were centrifuged at 800×g for 10 min at 4°C. Protein concentration was estimated in cell lysate supernatants, conditioned media and AH samples using the Bio-Rad protein assay reagent (C. No. 500-0006, Bio-Rad, Hercules, CA, USA). Samples containing equal amounts of proteins (10 μg for both cell lysates and CM) were mixed with Laemmli sample buffer and separated by sodium dodecyl sulfate-polyacrylamide gel electrophoresis (SDS-PAGE; with 10% or 12% acrylamide) and transferred to nitrocellulose membranes as we described earlier (Pattabiraman et al., 2014). AH samples also were processed as described above. Membranes were blocked for 2h at RT in TBS containing 0.1% Tween 20 and 5% (wt/vol) nonfat dry milk and subsequently probed with primary antibodies directed against VLK (rabbit polyclonal antibody;1:1000 dilution) and GAPDH (Glyceraldehyde-3-phosphate dehydrogenase; mouse monoclonal antibody; 1:5000 dilution; C. No. 60004-1-g, Proteintech Group, Inc. Rosemont, IL), in conjunction with horseradish peroxidase-conjugated secondary antibodies. Detection of immunoreactivity was based on enhanced chemiluminescence. Densitometric analysis of the immunoblots was performed using ImageJ software (http://imagej.nih.gov/ij/; provided in the public domain by the National Institutes of Health, Bethesda, MD, USA). Data were normalized to the specified loading controls.

For TyrP proteins, equal amounts (10 μg of protein) of the SDS-urea soluble ECM-enriched fractions derived from TM cells (Fig. 6B) subjected to various treatments and control conditions, were resolved on 4–20% SDS-PAGE gradient gels, transferred to nitrocellulose membranes and blocked with 1% BSA in PBS with 0.1% Tween 20 and probed with MultiMab rabbit mAb to phospho-Tyrosine (1:1000 dilution; C. No. P-Tyr-1000 from Cell Signaling Technology, Inc. Danvers, MA) or anti-rabbit fibronectin antibody (1:8000 dilution; obtained from Harold Erickson, Duke University, Durham. NC). Immunoreactivity was detected by enhanced chemiluminescence.

Extraction of ECM-enriched fraction

A step by step protocol describing the extraction of ECM-enriched protein fraction from TM cells is illustrated schematically in Fig. 6B. The protocol was based on the procedure described by Harvey et. al.(Harvey et al., 2013) with some modifications. Protein content of ECM-enriched fractions was quantified using the Pierce BCA Protein Assay Kit (ThermoFisher Scientific, Waltham, MA).

Silver staining of ECM proteins

After collection of conditioned media and detachment of cells using 0.25% Trypsin, the ECM retained on cell culture plates was incubated with 10% trichloroacid acid for 5 min, followed by washing with multiple changes of water. The washed ECM was then scraped using a cell lifter and dissolved in urea sample buffer containing 8 M urea, 20 mM Tris, 23 mM glycine, 10 mM dithiothreitol (DTT), and saturating concentration of sucrose along with protease and phosphatase inhibitors, and then sonicated. Protein concentrations were estimated by the Bradford protein assay(Bradford, 1976). Equal amounts (5 μg) of protein derived from the TGF-β2 treatment and respective control were separated on a gradient SDS-PAGE (4–20% Criterion XT precast gels) using 1× MOPs buffer (Invitrogen). The gels were fixed for 30 min at RT using a fix solution containing 10% methanol and 5% acetic acid in deionized water. Gels were washed thoroughly with several changes of deionized water, and incubated in sodium thiosulfate solution (0.8mg/100 ml) for 90 seconds. After a through washing with deionized water, gels were stained with silver nitrate solution (0.18mg/100ml) for approximately 10 min. After several washes with water, gels were treated with developer solution (20g of potassium carbonate, 40ml of sodium thiosulfate solution (0.8mg/100ml) and 500μl formaldehyde in 1 liter of water) for few seconds, following which development was immediately stopped by incubating gels in fix solution for 15 min. Silver stained gels were washed in deionized water prior to being imaged using a Fotodyne Trans illuminator.

Mass spectrometry

Sample preparation—For in-solution tryptic digestion, we employed the magnetic bead protocol as described by Hughes C.S. et. al.(Hughes et al., 2014). Briefly, ECM-enriched extracellular protein samples (25 μg protein) from both SDS-urea soluble and insoluble fractions (Fig. 6B) from control and TGF-β2 treatment were solubilized in 100 mM Tris-HCl (pH 6.8) buffer containing 2% SDS and 10 mM DTT (dithiothreitol), and alkylated with iodoacetamide (25mM) by incubating in dark at RT for 1 h, after which the reaction was quenched with 50 mM DTT. Fifty μl (10 μg/ml) of premixed paramagnetic beads (equal amounts of Sera-Mag™ SpeedBeads™ and Sera-Mag™ Carboxylate-Modified Magnetic Particles; GE Pharmaceuticals) were added to the alkylated protein preparation which was then acidified with 0.25% formic acid (pH <3), followed by an equal volume of 100% acetonitrile and incubation for 10 mins at RT. A magnetic rack was used to pull the beads to the wall and the supernatants were discarded, then beads were rinsed with 70% ethanol followed by acetonitrile. Trypsin/Lys-C mix (1μg; Promega. C. No. V5072) in 50 mM ammonium bicarbonate pH 8, was added and incubated overnight at 37 C. The following day, acetonitrile was added (>95%) to samples and incubated for 10 min. Samples were placed on the magnetic rack and supernatants discarded. Beads were rinsed again with acetonitrile and dried briefly for few minutes and 20 μl of 2% dimethyl sulfoxide and 0.2% formic acid was added to the beads and incubated for 5min. Supernatants were collected into a fresh tube, while the beads were incubated with 20 μl of 0.2% formic acid and incubated for 5min at RT and the supernatants were collected, vacuum-dried and dissolved in 10 μl of 0.1% trifluoroacetic acid containing 3% acetonitrile.

Liquid chromatography-tandem mass spectrometry (LC-MS-MS)

Tryptic digests (2 μl aliquots) were analyzed by LC-MS/MS using a nanoAcquity UPLC system coupled to a Synapt G2 HDMS mass spectrometer (Waters Corp, Milford, MA). Peptides were initially trapped on a 180 μm × 20 mm Symmetry C18 column (at the 5 μl/min flow rate for 3 min in 99.9% water, 0.1% formic acid). Peptide separation was then performed on a 75 μm × 150 mm column filled with the 1.7 μm C18 BEH resin (Waters) using a 6 to 30% acetonitrile gradient with 0.1% formic acid for 2 h at the flow rate of 0.3 μl/min at 35°C. Eluted peptides were sprayed into the ion source of Synapt G2 using the 10 μm PicoTip emitter (Waters) at the voltage of 3.0 kV.

Duplicate data-independent analyses (HDMSE) for each sample were conducted in similar LC settings for simultaneous peptide quantitation and identification. For robust peak detection and alignment of individual peptides across all HDMSE runs, automatic alignment of ion chromatography peaks representing the same mass/retention time features was performed using Progenesis QI software. To perform peptide assignment to the features, PLGS 2.5.1 (Waters Inc.) was used to generate searchable files that were submitted to the IdentityE search engine incorporated into Progenesis QI for Proteomics. For peptide identification, we searched against UniProt human database (2015 release). Protein abundances were calculated from the sum of all unique peptide ion intensities normalized by the intensities of all proteins in experimental samples. Conflicting peptides for different proteins and their isoforms were excluded from the calculations.

Statistical analysis

Data from immunoblot quantification were analyzed by the Student's t-test and a $P<0.05$ was considered to define statistically significant differences between test and control samples. Values are presented as mean ± Standard error of the mean (SEM). For ECM quantitative proteomics, ANOVA (analysis of variance) scores were calculated according to the Progenesis algorithm to compare changes between control and TGF-β2 treated samples.

Results

Expression and distribution pattern of a 32 kDa VLK isoform in human trabecular meshwork cells

The trabecular meshwork is considered to be mesenchymal in terms of developmental origin (Smith et al., 2001), and VLK is known to be expressed and distributed in the E-cadherin absent mesenchyme (Kinoshita et al., 2009). We employed multiple approaches to determine the expression and distribution pattern of VLK in primary human TM cells including RT-PCR amplification of VLK mRNA (NCBI: NM_138370.2) using VLK specific oligonucleotide primers (set 1: exon 1; set 2: exon 1/2; set 3: exon 1/4; set 4: exon 3/5 and set 5: exon 5/7), immunoblot and immunofluorescence analyses using a polyclonal antibody raised against a 15 amino acid peptide located mid-way in the primary amino acid sequence of the human VLK protein. RT-PCR analysis of RNA derived from human TM cells (isolated from two individual donor eyes from subjects aged 19 and 67 years) yielded amplification of the expected DNA products with primer sets 3, 4 and 5, but no detectable products with primer set 1 and 2 (Fig. 1A). The RT-PCR derived DNA products were

confirmed to be specific to VLK based on nucleotide sequencing. Similar results were observed with RNA derived from the human donor TM tissue as well (data not shown). Polyclonal VLK antibody detected a prominent species approximately ~32 kDa in conditioned media (10 μg protein) and lysates (800xg supernatants; 10 μg protein) of human TM cells derived from donor eyes of subjects aged 19, 23 and 69 years, as shown in Figure 1B. Two weaker immunopositive bands of approximately ~60 kDa and ~120 kDa were also detected by immunoblot analysis of TM cell lysates (Fig. 1B).

Additionally, immunofluorescence analysis of human TM cells (cultured on glass coverslips coated with 2% gelatin) using VLK polyclonal antibody in conjunction with secondary antibody conjugated to Alexa flour 568 revealed a characteristic distribution pattern, with VLK staining enrichment at the perinuclear and Golgi/endoplasmic reticulum regions (indicated with arrows in Fig. 1C). The distribution profile of VLK was also examined in tissues of the AH outflow pathway of human donor eyes by immunofluorescence analysis. As shown in Figure 1D, VLK immunostaining is detectable throughout the AH outflow pathway including in the TM, Schlemm's canal (SC) and juxtacanalicular tissues (JCT). In both TM cells (Fig. 1C) and tissue specimens (Fig.1D), nuclei were stained with Hoechst 33342 (blue staining). Tissue sections and TM cells stained with an Alexa fluor 568 conjugated secondary antibody alone did not exhibit detectable background or nonspecific immunostaining (data not shown). Since VLK is a known secreted protein (Bordoli et al., 2014), we checked for its presence in AH samples of human (cataract patients aged 55 and 72 years old; 15 μg protein) and porcine (10 & 50 μl, from freshly enucleated eyes obtained from a local slaughterhouse) origin, and detected a robust immunopositive band of approximately 32 kDa, similar to the results obtained by immunoblotting analysis of CM from human TM cells (Fig. 1E).

Regulation of VLK expression and secretion in human TM cells

To understand the regulation of VLK expression and secretion in TM cells, we explored the effects of dexamethasone, TGF-β2 and constitutively active RhoA, all of which have been shown to increase resistance to AH outflow and lead to increases in IOP (Clark et al., 1995; Fleenor et al., 2006; Pattabiraman et al., 2015). Treatment of confluent human TM cells with dexamethasone (0.5 μM) daily for 96 h under serum free condition stimulated a robust and significant increase in VLK protein levels (Fig. 2) in both, cell lysates (n=6; *P>0.05) and CM (n=6; *P<0.05%), relative to controls. Figures 2A and B depict representative immunoblots showing the changes in VLK protein levels in TM cell lysates (10 μg protein) and CM (10 μg protein), respectively, derived from dexamethasone (500 nM) treated (D1–D3) and control (C1 & C2) cells. GAPDH was immunoblotted as a loading control. Figures 2C and D show quantitative changes in the VLK protein levels (based on densitometric analysis) in TM cell lysates and CM from dexamethasone treated and control cells, respectively. For a loading control (Lcontrol; Fig. 2B) for the CM protein fraction, equal amounts of protein were separated by 10% SDS-PAGE and stained with Coomassie Brilliant Blue. A 55kDa protein whose levels were found to be identical based on staining between the treated and untreated samples was used for normalization. Values are presented as mean ±SEM.

Serum starved human TM cells treated for 96 h with TGF-β2 (4ng/ml), the levels of which have been reported to be elevated in the AH of primary open angle glaucoma (Tripathi et al., 1994), led to a significant (*P<0.05; Fig. 2) and progressive increase in VLK protein levels in both cell lysates (E &F) and CM (G&H). In cell lysates, the increase in VLK protein was evident at 8 h post TGF- β2 addition, continuing up to 72 h and plateauing by 96 h, compared to untreated controls (n=6, *P<0.05). In CM, the increase in VLK protein continued up to 24 h and plateaued by 72 h compared to controls (n=7, *P<0.05). Figures 2E & F (cell lysates) and G&H (CM) depict representative immunoblotting analyses of changes in VLK protein levels in TGF-β2 treated and control HTM cells (C1 & C2). Figures 2I &J show quantitative changes in VLK protein levels (presented as percent change) in cell lysates and CM, respectively, in TGF-β2 treated versus control HTM cells.

In addition to the effects of external cues described above, we also examined the effects of a constitutively activated RhoA GTPase on VLK expression in TM cells. Sustained activation of Rho GTPase in the AH outflow pathway has been reported to increase resistance to AH outflow and IOP in association with altered ECM production and TM contraction (Pattabiraman et al., 2015; Zhang et al., 2008). Expression of a constitutively active mutant of RhoA GTPase (adenovirally encoded RhoAV14) in human TM cells as described earlier (Zhang et al., 2008) revealed no significant changes in VLK protein levels in cell lysates at 36 h post transfection under serum free conditions (Figs. 3A & 3C). However, under these conditions, there was a significant (n=7, *P<0.05) increase in VLK protein levels in the CM of RhoAV14 expressing cells compared to GFP expressing control cells (Figs. 3B & 3D). Figures 3A & 3B depict representative VLK immunoblots of cell lysates and CM, respectively, derived from RhoAV14/GFP and GFP expressing TM cells. Figures 3C & 3D show quantitative changes in the VLK protein levels in RhoAV14/GFP expressing human TM cells (percent change based on densitometric analysis) relative to GFP expressing controls.

TM tissue is sensitive to mechanical stretch resulting from elevated IOP. Changes in mechanical stretch are known to elicit alterations in gene expression and secretion of various factors, by the TM cells and thought to play a role in maintenance of a steady state IOP and AH outflow (Borras, 2003; Luna et al., 2009; Vittal et al., 2005). Therefore, to determine the potential influence of cyclic mechanical stretch on VLK secretion by TM cells, human TM cells grown on type I collagen-coated flexible silicone sheets were subjected to cyclic mechanical stretch (20% stretch, cycle per second) for 48 h under serum free conditions. TM cells subjected to cyclic mechanical stretch exhibited a robust and significant (n=6, *P<0.05) increase in VLK protein levels in the CM as compared to untreated cells maintained under similar culture conditions (Fig.3). Figure 3E shows a representative immunoblot of VLK in CM derived from human TM cells subjected to cyclic mechanical stretch and control cells. Figure 3F shows quantitative changes in VLK protein levels (expressed as percent change based on densitometric analysis) in the CM of TM cells subjected to cyclic stretch relative to control cells.

Role of VLK in maintenance of TM cell shape, and formation of actin stress fibers and focal adhesions

To explore the role of VLK in TM cells, we studied the effects of VLK deficiency using an siRNA-based approach to suppress VLK gene expression. Human TM cells transfected with the siRNA pool containing three sets of VLK-specific small interfering RNAs, together with a scrambled siRNA control and cultured in 6 well plates for 72 h showed a nearly 60–70% decrease (n=12) in VLK protein levels in cell lysates (Figs. 4A & 4C) and CM (Figs. 4B & 4D) based on immunoblot analysis with subsequent quantification by densitometric analysis. Interestingly, suppression of VLK expression in TM cells maintained under 4% serum (for 72 h) was accompanied by a dramatic change in cell shape as shown in Figure 4E. Unlike cells treated with scrambled siRNA, the VLK siRNA treated cells exhibited a relaxed and retractile morphology (Fig. 4E). Consistent with these morphological changes, the VLK deficient cells also showed a dramatic decrease in actin stress fibers and focal adhesions based on rhodamine-phalloidin fluorescence (red) and vinculin immunofluorescence staining (green), respectively (Fig. 4F). Moreover, the VLK siRNA treated cells exhibited a marked reduction in immunofluorescence staining for phospho-tyrosine and phopsho-paxillin antibodies relative to scrambled siRNA treated controls, indicating a disruption in cell adhesive interactions under VLK deficiency (Fig. 4F). Cell nuclei (blue staining) were stained with Hoechst 33342 in the siRNA treated cells.

VLK deficiency decreases Tyrosine phosphorylation (TyrP) of ECM proteins derived from TM cells

To explore a role of VLK in TyrP of ECM proteins secreted by human TM cells, cells were first transfected with VLK siRNA and after 72 h; the ECM protein fraction was isolated as described in the Methods section. To rule out cellular contamination during the ECM extraction process, we always examined the ECM fraction attached to the cell culture plates under phase contrast microscopy following cell detachment (data not shown). Cells treated with scrambled siRNA served as controls. Equal amounts (10 μg) of ECM protein (SDS-urea soluble) derived from the VLK and scrambled siRNA treatments were separated on SDS-PAGE (4–20% gradient) and immunoblotted for TyrP proteins using MultiMab phospho-Tyrosine rabbit mAb (P-Tyr-1000) and blots were developed by chemiluminescence. As shown in Figure 5A, VLK siRNA treated samples showed a dramatic decrease (by ~80%) in TyrP of different ECM proteins with molecular mass ranging from 50 to >250 kDa, compared to scrambled siRNA treated cells. Lanes 1 to 4 in Figure 5A represent four independent samples from both control and VLK siRNA treatments. For loading controls, we used staining intensity of a 250 kDa protein from the ECM protein fraction (C; based on SDS-PAGE and Coomassie Brilliant Blue staining), and that for fibronectin immunoblotting (D). Figure 5B shows quantitative changes in the levels of TyrP proteins derived from the VLK siRNA and scrambled siRNA treated TM cells with a significant decrease in the VLK siRNA treated samples (n=8, *P<0.05), based on densitometric analysis (presented as percent change from controls).

Identification of TGF-β2 induced ECM proteins in human TM cells by proteomics analysis

Elevated levels of TGF-β2 are a consistent observation in the AH derived from glaucoma patients (Braunger et al., 2015; Tripathi et al., 1994), and elevated TGF-β2 was demonstrated to induce ocular hypertension in association with accumulation of ECM proteins in various experimental models (Braunger et al., 2015; Fleenor et al., 2006). However, there exists no comprehensive data on the effects of TGF-β2 at the level of expression profiles of ECM and ECM-associated proteins of TM cells. Therefore we determined the influence of TGF-β2 on the ECM protein profile of human TM cells by proteomics analysis. Prior to quantitative proteomics analysis, we evaluated TGF-β2-induced changes in the profile of ECM and ECM-associated proteins in HTM cells using SDS-PAGE and silver staining analysis. For this, human TM cells grown to confluence in plastic cell culture plates were serum starved for 24 h and treated with TGF-β2 (4 ng/ml) for 96 h. Following this, the ECM-enriched protein fraction was extracted from both controls and TGF-β2 treated cells as described in the Methods section under silver staining of ECM. Equal amounts (5 μg) of protein were separated by SDS-PAGE (4–20% gradient gel) and silver stained. Figure 6A shows a representative image of the ECM protein profile of TM cells (from two independent samples). As can be seen from the photograph, there was a detectable increase in protein staining intensity in TGF-β2 treated samples compared to the controls.

Following these preliminary observations, we repeated these studies and performed quantitative proteomics using label free protein quantification based on peptide intensities. To this end, we used a protocol described schematically in Fig. 6B to extract the ECM-enriched protein fraction. Supplemental Tables S1 and S2 list all the proteins identified in the ECM protein fraction derived from the SDS-urea soluble and insoluble fractions of TM cells, respectively (maintained under serum free conditions for 96 h), based on mass spectrometry analysis. Identification of proteins listed in these tables was based on a minimum of 2 peptides with > 99.9 confidence. Gene Ontology based on Panther protein category analysis identified ECM, receptor, defense/immunity and cytoskeletal proteins as some of the predominant constituents in both SDS-urea soluble and insoluble fractions (Supplemental Fig. S1).

Tables 1 and 2 list the ECM proteins whose levels were elevated by a minimum of 1.5 and 2-fold in the SDS urea soluble and urea insoluble fractions, respectively in the TGF-β2 treated human TM cells compared to controls. The results were based on three independent experiments. Importantly, as shown in Tables 1 and 2, the levels of several different ECM proteins and ECM-associated proteins including collagen, fibulins, fibronectin, laminin, elastin, lysyl oxidase, latent TGFβ binding protein 1, EGF-containing fibulin-like ECM proteins, matrix Gla protein, Tenascin, galactin-3-binding protein, clusterin, TGF-β induced bigh3, periostin and other proteins were significantly elevated in the TGF-β2 treated cells.

Role of VLK in the TGF-β2 induced TyrP of ECM proteins derived from TM cells

To understand whether TGF-β2 has additional effects on ECM proteins, we then evaluated the TyrP status of human TM cell ECM proteins. Human TM cells serum starved for 24 h and treated with TGF-β2 (4 ng/ml) for 48 h showed a significant increase (by ~70%; n=4,

*P<0.05) in the levels of TyrP of ECM proteins compared to control cells based on immunoblotting analysis (Fig. 7A; lanes 1 & 2 are two independent samples; arrows point to prominent differences) and densitometric quantification (Fig. 7B). We then proceeded to determine the effects of siRNA-mediated VLK deficiency on the TGF-β2 induced TyrP of ECM proteins of TM cells. For this, human TM cells were first treated with VLK siRNA or scrambled siRNA as described earlier, followed by addition of TGF-β2 (4ng/ml) after a 24 h period. Forty eight hours following the addition of TGF-β2, the ECM protein fraction was extracted and analyzed for TyrP levels by immunoblot analysis. As shown previously in Figure 5, suppression of VLK caused a dramatic reduction in TyrP of ECM proteins derived from the TM cells relative to controls treated with scrambled siRNA (Fig. 7C). Moreover, VLK deficiency also significantly decreased the TGF-β2-induced increase in levels of TyrP of ECM proteins relative to the corresponding controls (TM cells treated with TGF-β2 and scrambled siRNA). Duplicate representative samples are shown in Figure 7C for each treatment. Figure 7D shows quantitative changes in the levels of TyrP of ECM proteins in the various tests and control samples described above (n=8; *P<0.05). Panel E in Figure 7 shows a loading control based on SDS-PAGE gel staining of the ECM protein fraction with Coomassie Brilliant Blue staining. It should be noted that the effects of TGF-β2 on TyrP status of ECM proteins in the siRNA experiments is not as robust as those observed in serum starved cells (Fig. 7A) since the TM cells in the siRNA studies were maintained in 4% serum.

Discussion

Our primary goal in this study was to determine whether ECM and ECM-associated secretory proteins of TM cells are phosphorylated by VLK, to gauge the effects of VLK on TM cell behavior, and seek insights into the regulation of VLK expression and secretion in the context of homeostasis and dysregulation of AH outflow and IOP. Our results derived from cell culture studies demonstrate that human TM cells secrete a 32 kDa isoform of VLK, the expression of which is upregulated by TGF-β2, dexamethasone, RhoA and cyclic mechanical stretch. Most significantly, decreased TyrP of human TM cell ECM proteins under conditions of VLK deficiency was associated with a dramatic change in cell shape in conjunction with decreased formation of actin stress fibers and focal adhesions. These observations offer important molecular insights into the potential role of VLK-mediated TyrP of ECM and other secretory proteins in regulation of the contractile and adhesive properties of TM cells, which are recognized to influence AH outflow and IOP. To the best of our knowledge this is the first report on the role of VLK in regulating TyrP of ECM and ECM-associated proteins in TM cells, and on cellular events known to underlie ECM organization and AH outflow.

ECM production, turnover and compliance in tissues of the AH outflow pathway has been demonstrated to influence AH outflow and IOP by regulating the adhesive interactions, contractile and mechanical properties of TM cells (Oh et al., 2013; Pattabiraman and Rao, 2010; Raghunathan et al., 2013; Russell and Johnson, 2012; Vranka et al., 2015; Zhou et al., 2012). To investigate our hypothesis regarding the possible influence of ECM protein phosphorylation on regulating TM cell behavior, we focused in this study on VLK, a secretory atypical kinase which has been demonstrated to regulate TyrP of ECM, MMPs and

other secretory proteins (Bordoli et al., 2014). VLK, an N-glycosylated protein with a conserved signal sequence at the N-terminal region and a putative kinase domain spanning the C-terminal half of the molecule, is composed of 493 amino acids and an expected molecular mass of ~53–56 kDa (Bordoli et al., 2014; Kinoshita et al., 2009). Interestingly however, the polyclonal antibody used in this study consistently detected a prominent immunopositive band at around 32 kDa in both TM cell lysates and CM. This antibody has been shown to recognize two prominent species resolved by SDS-PAGE, with molecular mass of approximately 56 kDa and 32 kDa in human lung tissue (Origene, antibody data sheet). In the human liver hepatoma HepG2 cell line the same antibody detects predominantly a 56 kDa protein (Bordoli et al., 2014). Therefore, it is possible that the alternatively spliced 32 kDa species is the prominent isoform of VLK expressed in human TM cells. Consistent with the results from immunoblot analysis, RT-PCR analysis of VLK expression in human TM cells and tissue using primer sets 3, 4 and 5 spanning sequences between exon 1 to 7 yielded DNA products of expected size. This was not the case with primer sets 1 and 2, which were intended to cover the coding region of VLK starting from nucleotide 210 to 638 (exon 1) and 240 to 840 (exon 1/ 2), since these primer sets did not generate detectable RT-PCR product. Moreover, the siRNA–based suppression of VLK expression significantly reduced levels of the 32 kDa protein recognized by the anti-VLK polyclonal antibody in both cell lysates and CM, and as expected, VLK localization in TM cells was found to be abundantly distributed to the Golgi and endoplasmic reticulum (Bordoli et al., 2014). Based on these different observations, we conclude that human TM cells and tissue predominantly express a 32 kDa VLK isoform protein.

Some of the novel observations made in this study include the finding that VLK expression in TM cells is regulated by TGF-β2, dexamethasone, RhoA and cyclic mechanical stretch. Although VLK deficiency has been found to cause embryonic lethality in mice, indicating the requirement of this kinase for morphogenesis and survival (Imuta et al., 2009; Kinoshita et al., 2009), little is known about the regulation of VLK expression. In this study, we were particularly interested in understanding the expression of VLK in TM cells by agents that have been confirmed to influence AH outflow and IOP via effects on ECM homeostasis. The agents tested in this study including TGF-β2, dexamethasone, constitutively active RhoA and mechanical stretch which increased the levels of VLK protein in the CM of TM cells, have been shown to modulate AH outflow indicating a possible involvement of VLK in AH outflow and IOP changes in both normal and glaucomatous eyes. In the case of human TM cells treated with TGF-β2 and dexamethasone, VLK protein levels were significantly increased in cell lysates as well, indicating an upregulation of VLK expression. Intriguingly, a similar response was not observed in RhoAV14 expressing TM cells suggesting the increased levels of VLK in the CM of TM cells expressing RhoAV14 might be the result of actin cytosketal reorganization and the subsequent influence of this event on the secretory pathway (Wang and Thurmond, 2009; Zhang et al., 2008). Further studies are required, however, to monitor time-dependent changes in VLK expression and secretion under conditions involving sustained activation of RhoA. It is also not known whether the observed increase in the levels of VLK in CM from TM cells subjected to mechanical stretch is due to increased expression, since we did not evaluate the levels of VLK protein in lysates from these cells. We have also not tested whether the different agents used in this study also

regulate VLK phosphorylation, which is required for the secretion of this kinase (Bordoli et al., 2014). However, our results reveal that VLK expression and secretion can be regulated by both, various external cues and intracellular signaling proteins. In a broader context, this information is significant since our knowledge in general regarding the regulation and role of ectokinases including VLK is only in its infancy (Bordoli et al., 2014; Tagliabracci et al., 2013).

By far the most important observation from this study concerns the dramatic effects of siRNA-induced deficiency of VLK protein in TM cells on cell shape in association with decreased levels of actin stress fibers and focal adhesions, and the correlation of these changes with decreased TyrP of ECM and ECM-associated proteins. TM cells plated on the ECM protein coated glass coverslips or stimulated with TGF-β2 and dexamethasone have been demonstrated to exhibit changes in contractile activity, actin cytoskeletal crosslinking, actin stress fiber and focal adhesion formation, cell stiffness and paracellular permeability (Clark et al., 2005; Gagen et al., 2014; Li et al., 2004; Pattabiraman and Rao, 2010; Raghunathan et al., 2015; Tian et al., 2000; Zhang et al., 2008). These changes are presumed to directly modulate AH outflow and IOP (Gagen et al., 2014; Rao et al., 2001; Tian et al., 2000). What is not entirely understood is the regulation of instructive signaling mechanisms harnessed by the ECM to modulate TM cell function and behavior. Therefore, our data on the effects of VLK deficiency on TyrP of ECM proteins of TM cells, and subsequent changes in cell shape and decreased actin stress fibers and focal adhesions mimic those of Rho kinase inhibitors and actin depolymerizing agents such as latrunculin and cytochalasin-D which are known to lower IOP via increasing AH outflow(Rao et al., 2001; Tian et al., 2000), and suggest that VLK inhibition may very well increase AH outflow and lower IOP by regulating ECM TyrP. Importantly, these observations also offer novel molecular insights into the role of ECM phosphorylation in homeostasis of AH outflow and IOP and open up the possibility that posttranslational modification of ECM proteins via TyrP represents an additional level of regulation in this process. In addition to regulating integrin-mediated outside-in signaling in TM cells, TyrP of ECM, MMPs and matricellular proteins may also influence ECM organization, stiffness, turnover and bioavailability of growth factors such as TGF-β. Therefore, small molecular compounds that selectively inhibit VLK might possess IOP lowering activity with potential for therapeutic use in glaucoma patients. Importantly, such novel VLK inhibitors may lower IOP by increasing AH outflow through both the conventional as well as uveo-scleral pathways. It is noteworthy that in Xenopus, PKDCC/VLK has been shown to regulate Wnt/PCP signaling which influences actin cytoskeletal organization and cell adhesion (Vitorino et al., 2015). Involvement of Wnt signaling in regulation of actin cytoskeletal organization, cell adhesion, AH outflow and IOP is well recognized (Kwon et al., 2009a; Wang et al., 2008; Yuan et al., 2013), suggesting a possible functional interaction between VLK and Wnt in the AH outflow pathway.

Finally, our results also demonstrate that TGF-β2 stimulates the accumulation and TyrP of various ECM proteins in TM cells. Importantly, VLK deficiency significantly reduced TGF-β2 induced TyrP of ECM and ECM –associated proteins in TM cells. These observations, together with the effects of TGF-β2 on VLK expression, further support a role for VLK in growth factor mediated, ECM-induced effects on TM cell behavior. Although we have not tested the possibility, it is reasonable to speculate that TGF-β2-mediated increases in VLK

expression and secretion could be partly responsible for increased TyrP of ECM proteins of TM cells by TGF-β2. Since an elevated level of TGF-β2 is a common finding in the AH of human glaucoma patients (Braunger et al., 2015; Tripathi et al., 1994), it is possible that TGF-β2-mediated dysregulation of VLK expression is part of the pathogenic cascade leading to impairment of outflow and elevated IOP. We anticipate that future studies to isolate TyrP ECM and ECM-associated proteins through affinity pulldown assays and identification of individual ECM proteins by mass spectrometry can lead to a mechanistic understanding of the role of different TyrP extracellular proteins, including the ECM, matricellular proteins and MMPs, and of VLK in TM cell biology and homeostasis of AH outflow. Moreover, it would be also interesting to explore whether any of the currently used IOP lowering drugs act partly by modulating VLK activity.

Based on the VLK data from our studies, it is conceivable that Fam20C might also play a role in the AH outflow pathway. Fam20C is another well characterized ectokinase which regulates serine phosphorylation of various ECM and other extracellular proteins, and has been shown to play a crucial role(s) in both physiological and pathological processes (Cui et al., 2015; Tagliabracci et al., 2012; Tagliabracci et al., 2013; Tagliabracci et al., 2015; Yalak and Vogel, 2012; Yalak and Vogel, 2015). TM cells are confirmed to express Fam20A, 20B and 20C based on RT-PCR analyses (our unpublished data) which coordinately regulate serine phosphorylation of different extracellular proteins (Cui et al., 2015). Collectively, the results of this study on regulation of VLK expression in TM cells and its role in controlling TyrP of ECM proteins, and associated effects on cell behavior expand our knowledge of the potential physiological and pathological importance of ectokinases and ectophosphatases in ECM biology and support the case for further exploration of the physiological role of these enzymes.

Supplementary Material

Refer to Web version on PubMed Central for supplementary material.

Acknowledgments

Contract grant sponsor- The National Institutes of Health

Contract grant numbers-R01EY018590; R01EY025096; P30-EY-005722

We thank Patrick Casey and Harold Erickson from Duke University for providing the adenovirus expressing RhoAV14 and GFP, and fibronectin polyclonal antibody, respectively. We also thank Pratap Challa, glaucoma specialist for providing the human aqueous humor samples used in this study. This work was supported by the National Institutes of Health Grants to P. V. R (R01-EY-018590 and R01-EY-025096) and the National Eye Institute Vision Core Grant P30-EY-005722.

Abbreviations Used

CM	Conditioned media
ECM	Extracellular matrix
GAPDH	Glyceraldehyde 3-phosphate dehydrogenase

JCT	Juxtacanalicular tissue
RT-PCR	Reverse transcriptase polymerase chain reaction
-RT	minus reverse transcriptase
SC	Schlemm's canal
SDS-PAGE	sodium dodecyl sulfate polyacrylamide gel electrophoresis
SEM	Standard error of the mean
siRNA	Small interfering RNA
TM	Trabecular meshwork
TyrP	Tyrosine phosphorylation
VLK	Vertebrate lonesome kinase
AH	Aqueous Humor

Literature Cited

Alvarado J, Murphy C, Juster R. Trabecular meshwork cellularity in primary open-angle glaucoma and nonglaucomatous normals. Ophthalmology. 1984; 91(6):564–579. [PubMed: 6462622]

Bill A. Conventional and uveo-scleral drainage of aqueous humour in the cynomolgus monkey (Macaca irus) at normal and high intraocular pressures. Experimental eye research. 1966; 5(1):45–54. [PubMed: 4160221]

Bordoli MR, Yum J, Breitkopf SB, Thon JN, Italiano JE Jr, Xiao J, Worby C, Wong SK, Lin G, Edenius M, Keller TL, Asara JM, Dixon JE, Yeo CY, Whitman M. A secreted tyrosine kinase acts in the extracellular environment. Cell. 2014; 158(5):1033–1044. [PubMed: 25171405]

Borras T. Gene expression in the trabecular meshwork and the influence of intraocular pressure. Progress in retinal and eye research. 2003; 22(4):435–463. [PubMed: 12742391]

Bradford MM. A rapid and sensitive method for the quantitation of microgram quantities of protein utilizing the principle of protein-dye binding. Analytical biochemistry. 1976; 72:248–254. [PubMed: 942051]

Bradley JM, Vranka J, Colvis CM, Conger DM, Alexander JP, Fisk AS, Samples JR, Acott TS. Effect of matrix metalloproteinases activity on outflow in perfused human organ culture. Investigative ophthalmology & visual science. 1998; 39(13):2649–2658. [PubMed: 9856774]

Braunger BM, Fuchshofer R, Tamm ER. The aqueous humor outflow pathways in glaucoma: A unifying concept of disease mechanisms and causative treatment. European journal of pharmaceutics and biopharmaceutics : official journal of Arbeitsgemeinschaft fur Pharmazeutische Verfahrenstechnik eV. 2015; 95(Pt B):173–181.

Bucolo C, Salomone S, Drago F, Reibaldi M, Longo A, Uva MG. Pharmacological management of ocular hypertension: current approaches and future prospective. Current opinion in pharmacology. 2013; 13(1):50–55. [PubMed: 23069477]

Clark AF, Brotchie D, Read AT, Hellberg P, English-Wright S, Pang IH, Ethier CR, Grierson I. Dexamethasone alters F-actin architecture and promotes cross-linked actin network formation in human trabecular meshwork tissue. Cell motility and the cytoskeleton. 2005; 60(2):83–95. [PubMed: 15593281]

Clark AF, Wilson K, de Kater AW, Allingham RR, McCartney MD. Dexamethasone-induced ocular hypertension in perfusion-cultured human eyes. Investigative ophthalmology & visual science. 1995; 36(2):478–489. [PubMed: 7843916]

Cohen P. The origins of protein phosphorylation. Nature cell biology. 2002; 4(5):E127–130. [PubMed: 11988757]

Cui J, Xiao J, Tagliabracci VS, Wen J, Rahdar M, Dixon JE. A secretory kinase complex regulates extracellular protein phosphorylation. eLife. 2015; 4:e06120. [PubMed: 25789606]

Fischer EH. Phosphorylase and the origin of reversible protein phosphorylation. Biological chemistry. 2010; 391(2–3):131–137. [PubMed: 20030590]

Fleenor DL, Shepard AR, Hellberg PE, Jacobson N, Pang IH, Clark AF. TGFbeta2-induced changes in human trabecular meshwork: implications for intraocular pressure. Investigative ophthalmology & visual science. 2006; 47(1):226–234. [PubMed: 16384967]

Gabelt BT, Kaufman PL. Changes in aqueous humor dynamics with age and glaucoma. Progress in retinal and eye research. 2005; 24(5):612–637. [PubMed: 15919228]

Gagen D, Faralli JA, Filla MS, Peters DM. The role of integrins in the trabecular meshwork. Journal of ocular pharmacology and therapeutics : the official journal of the Association for Ocular Pharmacology and Therapeutics. 2014; 30(2–3):110–120.

Gaton DD, Sagara T, Lindsey JD, Gabelt BT, Kaufman PL, Weinreb RN. Increased matrix metalloproteinases 1, 2, and 3 in the monkey uveoscleral outflow pathway after topical prostaglandin F(2 alpha)-isopropyl ester treatment. Archives of ophthalmology. 2001; 119(8): 1165–1170. [PubMed: 11483084]

Gerometta R, Spiga MG, Borras T, Candia OA. Treatment of sheep steroid-induced ocular hypertension with a glucocorticoid-inducible MMP1 gene therapy virus. Investigative ophthalmology & visual science. 2010; 51(6):3042–3048. [PubMed: 20089869]

Han H, Wecker T, Grehn F, Schlunck G. Elasticity-dependent modulation of TGF-beta responses in human trabecular meshwork cells. Investigative ophthalmology & visual science. 2011; 52(6): 2889–2896. [PubMed: 21282571]

Harvey A, Yen TY, Aizman I, Tate C, Case C. Proteomic analysis of the extracellular matrix produced by mesenchymal stromal cells: implications for cell therapy mechanism. PloS one. 2013; 8(11):e79283. [PubMed: 24244468]

Hughes CS, Foehr S, Garfield DA, Furlong EE, Steinmetz LM, Krijgsveld J. Ultrasensitive proteome analysis using paramagnetic bead technology. Molecular systems biology. 2014; 10:757. [PubMed: 25358341]

Imuta Y, Nishioka N, Kiyonari H, Sasaki H. Short limbs, cleft palate, and delayed formation of flat proliferative chondrocytes in mice with targeted disruption of a putative protein kinase gene, Pkdcc (AW548124). Developmental dynamics : an official publication of the American Association of Anatomists. 2009; 238(1):210–222. [PubMed: 19097194]

Junglas B, Yu AH, Welge-Lussen U, Tamm ER, Fuchshofer R. Connective tissue growth factor induces extracellular matrix deposition in human trabecular meshwork cells. Experimental eye research. 2009; 88(6):1065–1075. [PubMed: 19450452]

Kanski, JJ., Bowling, B., Nischal, KK., Pearson, A. Clinical ophthalmology a systematic approach. Edinburgh; New York: Elsevier/Saunders; 2011.

Keller KE, Aga M, Bradley JM, Kelley MJ, Acott TS. Extracellular matrix turnover and outflow resistance. Experimental eye research. 2009; 88(4):676–682. [PubMed: 19087875]

Kinoshita M, Era T, Jakt LM, Nishikawa S. The novel protein kinase Vlk is essential for stromal function of mesenchymal cells. Development. 2009; 136(12):2069–2079. [PubMed: 19465597]

Kwon HS, Lee HS, Ji Y, Rubin JS, Tomarev SI. Myocilin is a modulator of Wnt signaling. Molecular and cellular biology. 2009a; 29(8):2139–2154. [PubMed: 19188438]

Kwon YH, Fingert JH, Kuehn MH, Alward WL. Primary open-angle glaucoma. The New England journal of medicine. 2009b; 360(11):1113–1124. [PubMed: 19279343]

Li AF, Tane N, Roy S. Fibronectin overexpression inhibits trabecular meshwork cell monolayer permeability. Molecular vision. 2004; 10:750–757. [PubMed: 15496827]

Luna C, Li G, Liton PB, Epstein DL, Gonzalez P. Alterations in gene expression induced by cyclic mechanical stress in trabecular meshwork cells. Molecular vision. 2009; 15:534–544. [PubMed: 19279691]

Oh DJ, Kang MH, Ooi YH, Choi KR, Sage EH, Rhee DJ. Overexpression of SPARC in human trabecular meshwork increases intraocular pressure and alters extracellular matrix. Investigative ophthalmology & visual science. 2013; 54(5):3309–3319. [PubMed: 23599341]

Pattabiraman PP, Maddala R, Rao PV. Regulation of plasticity and fibrogenic activity of trabecular meshwork cells by Rho GTPase signaling. Journal of cellular physiology. 2014; 229(7):927–942. [PubMed: 24318513]

Pattabiraman PP, Rao PV. Mechanistic basis of Rho GTPase-induced extracellular matrix synthesis in trabecular meshwork cells. Am J Physiol Cell Physiol. 2010; 298(3):C749–763. [PubMed: 19940066]

Pattabiraman PP, Rinkoski T, Poeschla E, Proia A, Challa P, Rao PV. RhoA GTPase-induced ocular hypertension in a rodent model is associated with increased fibrogenic activity in the trabecular meshwork. The American journal of pathology. 2015; 185(2):496–512. [PubMed: 25499974]

Raghunathan VK, Morgan JT, Dreier B, Reilly CM, Thomasy SM, Wood JA, Ly I, Tuyen BC, Hughbanks M, Murphy CJ, Russell P. Role of substratum stiffness in modulating genes associated with extracellular matrix and mechanotransducers YAP and TAZ. Investigative ophthalmology & visual science. 2013; 54(1):378–386. [PubMed: 23258147]

Raghunathan VK, Morgan JT, Park SA, Weber D, Phinney BS, Murphy CJ, Russell P. Dexamethasone Stiffens Trabecular Meshwork, Trabecular Meshwork Cells, and Matrix. Investigative ophthalmology & visual science. 2015; 56(8):4447–4459. [PubMed: 26193921]

Rao PV, Deng PF, Kumar J, Epstein DL. Modulation of aqueous humor outflow facility by the Rho kinase-specific inhibitor Y-27632. Investigative ophthalmology & visual science. 2001; 42(5): 1029–1037. [PubMed: 11274082]

Russell P, Johnson M. Elastic modulus determination of normal and glaucomatous human trabecular meshwork. Investigative ophthalmology & visual science. 2012; 53(1):117.

Sethi A, Mao W, Wordinger RJ, Clark AF. Transforming growth factor-beta induces extracellular matrix protein cross-linking lysyl oxidase (LOX) genes in human trabecular meshwork cells. Investigative ophthalmology & visual science. 2011; 52(8):5240–5250. [PubMed: 21546528]

Simpson MA, Hsu R, Keir LS, Hao J, Sivapalan G, Ernst LM, Zackai EH, Al-Gazali LI, Hulskamp G, Kingston HM, Prescott TE, Ion A, Patton MA, Murday V, George A, Crosby AH. Mutations in FAM20C are associated with lethal osteosclerotic bone dysplasia (Raine syndrome), highlighting a crucial molecule in bone development. American journal of human genetics. 2007; 81(5):906–912. [PubMed: 17924334]

Smith RS, Zabaleta A, Savinova OV, John SW. The mouse anterior chamber angle and trabecular meshwork develop without cell death. BMC developmental biology. 2001; 1:3. [PubMed: 11228591]

Tagliabracci VS, Engel JL, Wen J, Wiley SE, Worby CA, Kinch LN, Xiao J, Grishin NV, Dixon JE. Secreted kinase phosphorylates extracellular proteins that regulate biomineralization. Science. 2012; 336(6085):1150–1153. [PubMed: 22582013]

Tagliabracci VS, Pinna LA, Dixon JE. Secreted protein kinases. Trends in biochemical sciences. 2013; 38(3):121–130. [PubMed: 23276407]

Tagliabracci VS, Wiley SE, Guo X, Kinch LN, Durrant E, Wen J, Xiao J, Cui J, Nguyen KB, Engel JL, Coon JJ, Grishin N, Pinna LA, Pagliarini DJ, Dixon JE. A Single Kinase Generates the Majority of the Secreted Phosphoproteome. Cell. 2015; 161(7):1619–1632. [PubMed: 26091039]

Tektas OY, Hammer CM, Danias J, Candia O, Gerometta R, Podos SM, Lutjen-Drecoll E. Morphologic changes in the outflow pathways of bovine eyes treated with corticosteroids. Investigative ophthalmology & visual science. 2010; 51(8):4060–4066. [PubMed: 20237246]

Tian B, Geiger B, Epstein DL, Kaufman PL. Cytoskeletal involvement in the regulation of aqueous humor outflow. Investigative ophthalmology & visual science. 2000; 41(3):619–623. [PubMed: 10711672]

Tripathi RC, Li J, Chan WF, Tripathi BJ. Aqueous humor in glaucomatous eyes contains an increased level of TGF-beta 2. Experimental eye research. 1994; 59(6):723–727. [PubMed: 7698265]

Vitorino M, Silva AC, Inacio JM, Ramalho JS, Gur M, Fainsod A, Steinbeisser H, Belo JA. Xenopus Pkdcc1 and Pkdcc2 Are Two New Tyrosine Kinases Involved in the Regulation of JNK Dependent Wnt/PCP Signaling Pathway. PloS one. 2015; 10(8):e0135504. [PubMed: 26270962]

Vittal V, Rose A, Gregory KE, Kelley MJ, Acott TS. Changes in gene expression by trabecular meshwork cells in response to mechanical stretching. Invest Ophthalmol Vis Sci. 2005; 46(8): 2857–2868. [PubMed: 16043860]

Vranka JA, Kelley MJ, Acott TS, Keller KE. Extracellular matrix in the trabecular meshwork: intraocular pressure regulation and dysregulation in glaucoma. Experimental eye research. 2015; 133:112–125. [PubMed: 25819459]

Wallace DM, Murphy-Ullrich JE, Downs JC, O'Brien CJ. The role of matricellular proteins in glaucoma. Matrix biology : journal of the International Society for Matrix Biology. 2014; 37:174–182. [PubMed: 24727033]

Wang WH, McNatt LG, Pang IH, Millar JC, Hellberg PE, Hellberg MH, Steely HT, Rubin JS, Fingert JH, Sheffield VC, Stone EM, Clark AF. Increased expression of the WNT antagonist sFRP-1 in glaucoma elevates intraocular pressure. The Journal of clinical investigation. 2008; 118(3):1056–1064. [PubMed: 18274669]

Wang Z, Thurmond DC. Mechanisms of biphasic insulin-granule exocytosis - roles of the cytoskeleton, small GTPases and SNARE proteins. Journal of cell science. 2009; 122(Pt 7):893–903. [PubMed: 19295123]

Weinreb RN, Khaw PT. Primary open-angle glaucoma. Lancet. 2004; 363(9422):1711–1720. [PubMed: 15158634]

Yalak G, Vogel V. Extracellular phosphorylation and phosphorylated proteins: not just curiosities but physiologically important. Science signaling. 2012; 5(255):re7. [PubMed: 23250399]

Yalak G, Vogel V. Ectokinases as novel cancer markers and drug targets in cancer therapy. Cancer medicine. 2015; 4(3):404–414. [PubMed: 25504773]

Yuan Y, Call MK, Yuan Y, Zhang Y, Fischesser K, Liu CY, Kao WW. Dexamethasone induces cross-linked actin networks in trabecular meshwork cells through noncanonical wnt signaling. Investigative ophthalmology & visual science. 2013; 54(10):6502–6509. [PubMed: 23963164]

Zhang M, Maddala R, Rao PV. Novel molecular insights into RhoA GTPase-induced resistance to aqueous humor outflow through the trabecular meshwork. American journal of physiology Cell physiology. 2008; 295(5):C1057–1070. [PubMed: 18799648]

Zhou EH, Krishnan R, Stamer WD, Perkumas KM, Rajendran K, Nabhan JF, Lu Q, Fredberg JJ, Johnson M. Mechanical responsiveness of the endothelial cell of Schlemm's canal: scope, variability and its potential role in controlling aqueous humour outflow. Journal of the Royal Society, Interface / the Royal Society. 2012; 9(71):1144–1155.

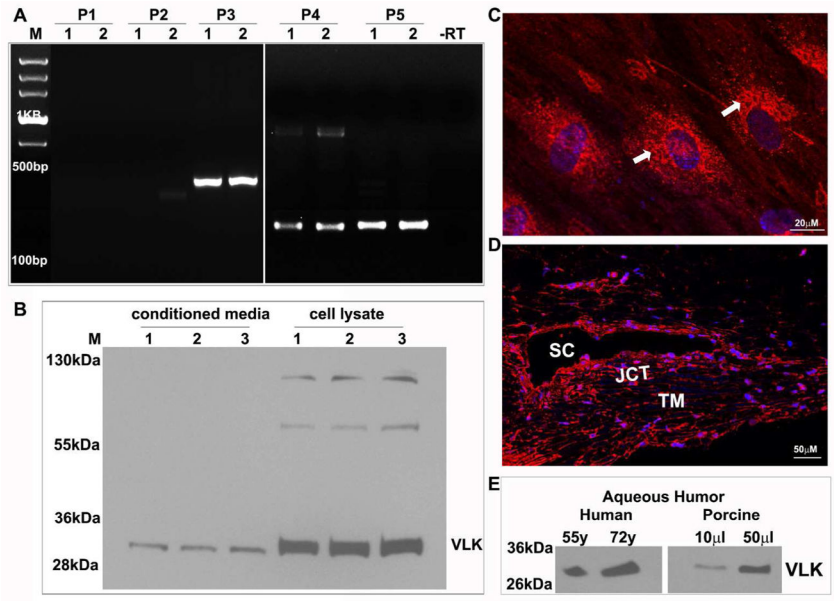

Figure 1.

Expression and distribution of VLK in human TM cells, tissue and aqueous humor. Confirmation of VLK expression in human TM cells (derived from two different donor eyes-lanes 1 & 2) by RT-PCR amplification (A). While VLK specific DNA products of the expected size were amplified with primer sets (P) 3, 4 & 5, no DNA product was detected using set 1 and 2 primers. Lane M depicts nucleotide bp markers; –RT; sample derived from the absence of reverse transcriptase. B. Immunoblotting analysis of VLK protein in TM cell lysates and conditioned media (CM) derived from three different samples (lanes 1–3) using VLK polyclonal antibody identified a prominent immunopositive species of approximately 32 kDa in both lysates and CM. C. Distribution of VLK (red) in TM cells by immunofluorescence shows a Golgi/endoplasmic reticulum specific localization (white arrows). D. Immunofluorescence-based analysis of VLK distribution in the human AH outflow pathway (paraffin sections) shows positive staining in the TM, and the Schlemm's canal (SC) and juxtacanalicular area (JCT). In panels C & D, the nuclei were stained with Hoechst 33342 (blue) and bars indicate image magnification. E. Detection of VLK in the AH of human and porcine by immunoblot analysis.

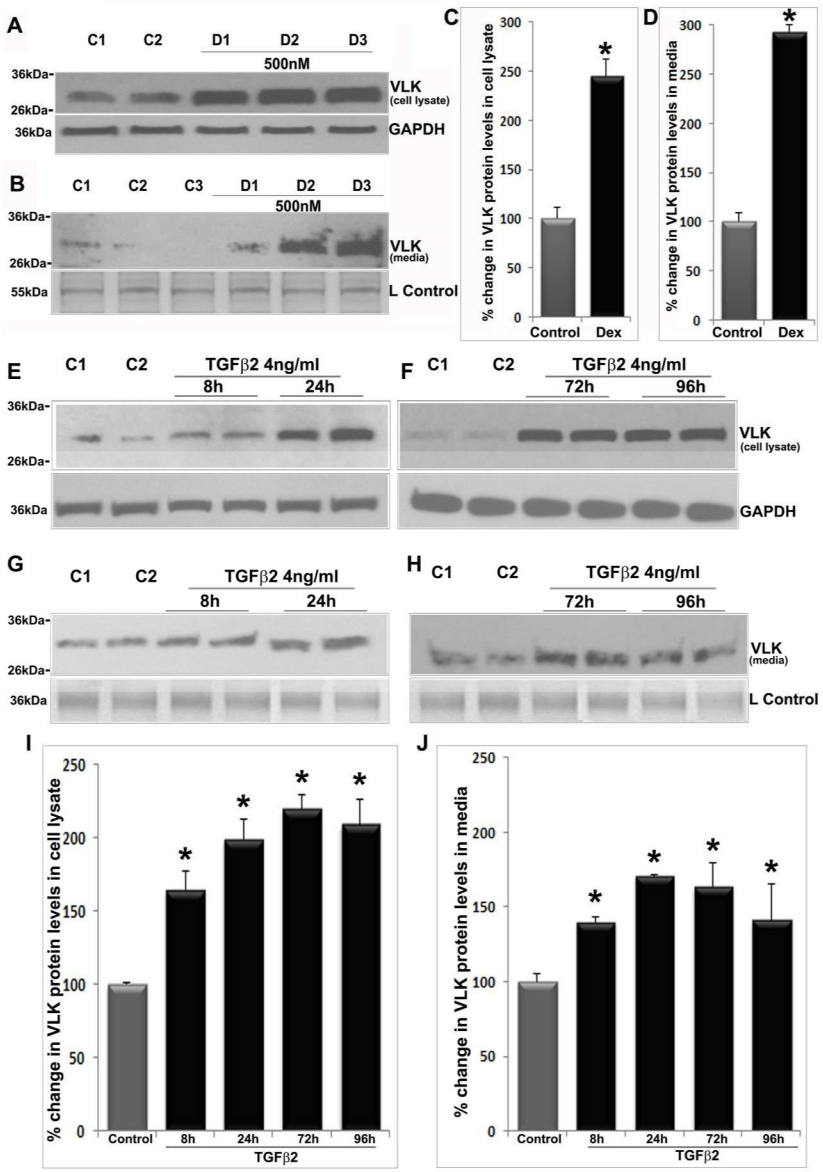

Figure 2.

Dexamethasone and TGF-β2 increase VLK protein levels in human TM cell lysates and conditioned media. Serum starved TM cells (derived from different donors; D1–D3) treated with dexamethasone (500 nM) consecutively for 96 h showed a significant increase in VLK protein levels in both cell lysates (A &C) and in CM (B&D), compared to control cells (C1–C2) based on immunoblotting analysis with subsequent densitometric quantification. N=6; *P<0.05. Serum starved TM cells treated with TGF-β2 (4 ng/ml) for 96 h showed a significant increase in VLK protein levels based on immunoblotting and densitometric quantification, starting from 8 h continuing until 72 h post-treatment, plateauing thereafter by 96 h in cell lysates (E, F & I; n=6; *P<0.05), and plateauing after 24 h in CM samples (G, H & J; n=7; *P<0.05) compared to control cells. Staining of 55 kDa (Panel B) and 36 kDa (Panel G&H) proteins based on SDS-PAGE and Coomassie blue present in the CM protein

samples was used as loading controls (L Control). GAPDH served as a loading control for cell lysate samples (A, E & F). Values are mean ±SEM.

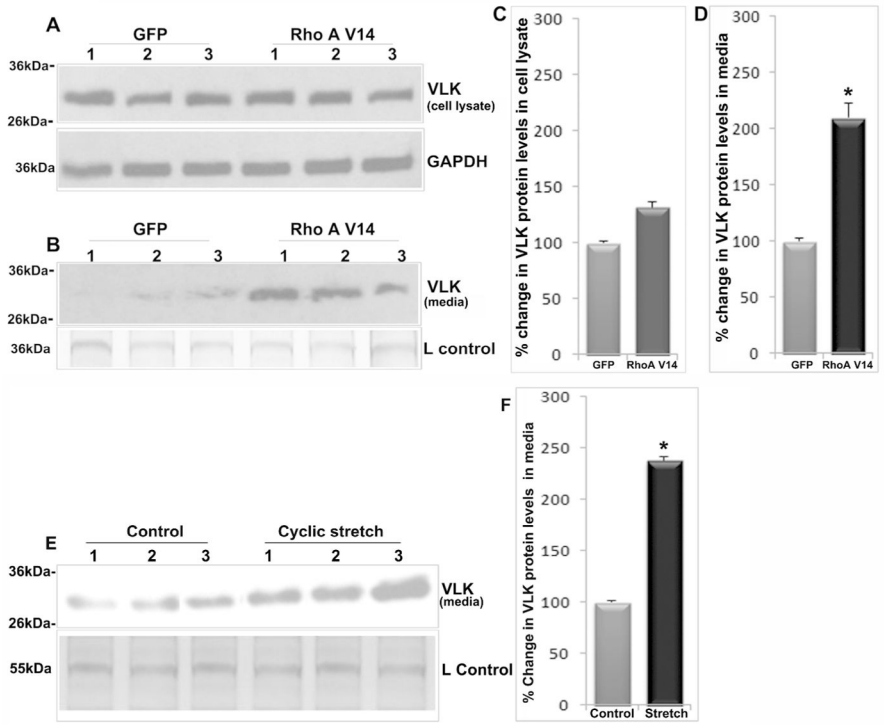

Figure 3.

RhoA activation and cyclic mechanical stretch increase VLK protein levels in human TM cell conditioned media. TM cells expressing a constitutively active RhoA (RhoAV14 mutant) for 36 h under serum free conditions exhibited significantly increased levels of VLK protein in the CM based on immunoblot analysis and densitometric quantification as compared to GFP expressing control cells (B&D). N=7, *P<0.05. VLK protein levels in TM cell lysates however, were found to be unaltered in cells expressing RhoAV14 (A&C; n=7). Lower panels in A & B show the loading controls. E& F. Subjecting TM cells (lanes 1–3 represent three independent samples) grown on type 1 collagen-coated silicone sheets to cyclic mechanical stretch (20% stretching, one cycle per second) for 48 h significantly increased VLK protein levels in the CM compared to control cells based on immunoblotting and densitometric analyses. N=6, *P<0.05. Loading control is shown in the lower panel of E. Values are mean ± SEM.

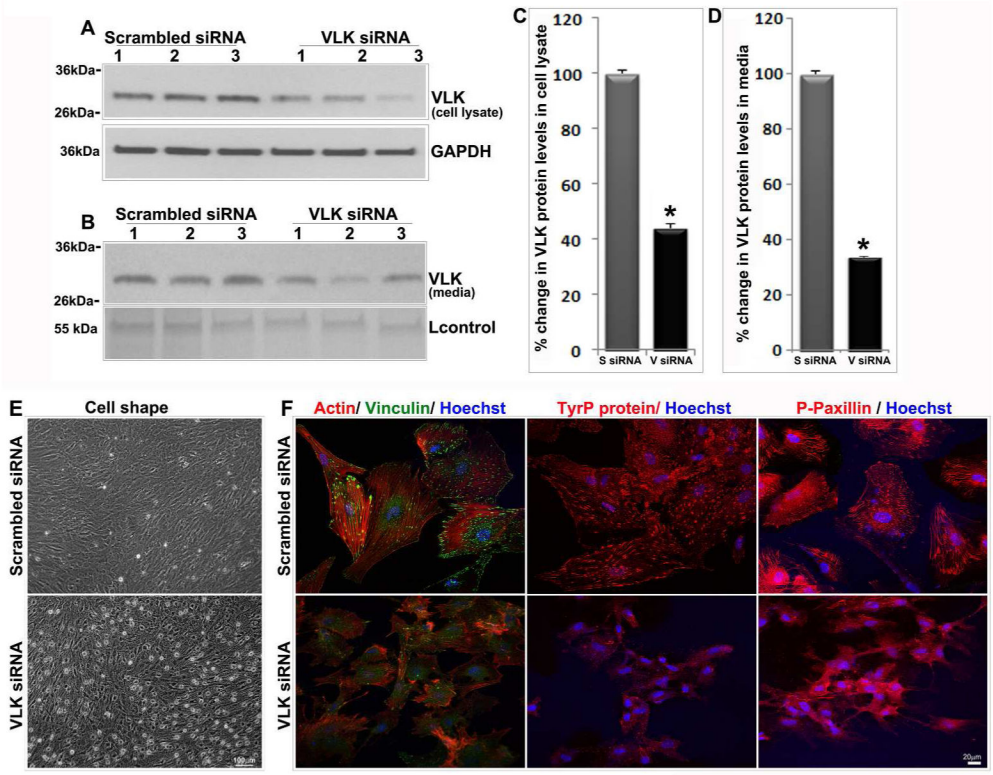

Figure 4.

VLK deficiency in human TM cells induces changes in cell shape and decreases in actin stress fibers and focal adhesions. TM cells (lanes 1–3 represent 3 individual samples) treated with siRNA specific to VLK for 72 h showed a significant decrease in VLK protein levels in both cell lysates (A & C) and media (B & D) compared to the control cells treated with scrambled siRNA, based on immunoblotting and densitometric analyses. Values are mean ± SEM of 12 independent analyses. *P<0.05. Lower panels in A & B show the loading controls. E. TM cells treated with VLK siRNA for 72 h reveal changes in cell shape by phase contrast microscopy compared to the control cells treated with scrambled siRNA. F. TM cells treated with VLK siRNA exhibit a decrease in actin stress fibers (Rhodamine-phallodine staining), focal adhesions (vinculin staining) and in phospho-tyrosine and phospho-paxillin immunofluorescence compared to control cells treated with scrambled siRNA. Bars in E & F show image magnification.

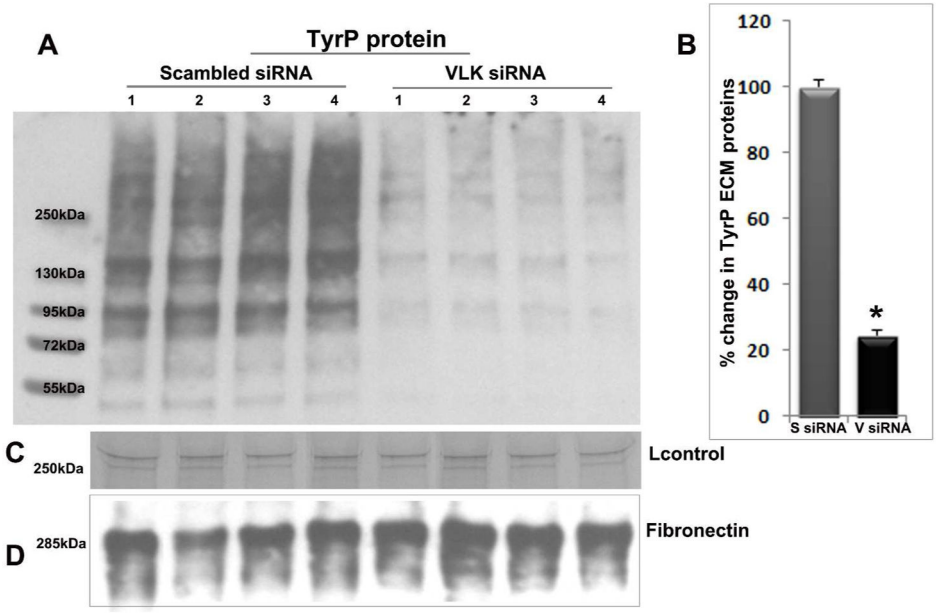

Figure 5.

VLK deficiency suppresses TyrP of ECM proteins secreted by human TM cells. A. The ECM-enriched extracellular protein fraction (SDS-urea soluble) derived from TM cells (lanes 1–4 represent 4 independent samples) treated with scrambled siRNA (S siRNA) for 72 h showed an intense immunostaining for TyrP proteins with molecular mass ranging from 50 to >250 kDa in immunoblots developed using MultiMab phospho-Tyrosine rabbit mAb. In contrast to the scrambled siRNA treated cells, TM cells treated with VLK-specific siRNA (V siRNA) demonstrated a dramatic and significant decrease in the levels of TyrP ECM proteins based on immunoblot quantification (A&B). Panels C and D show loading controls. Values are mean ±SEM of 8 independent samples. *P<0.05.

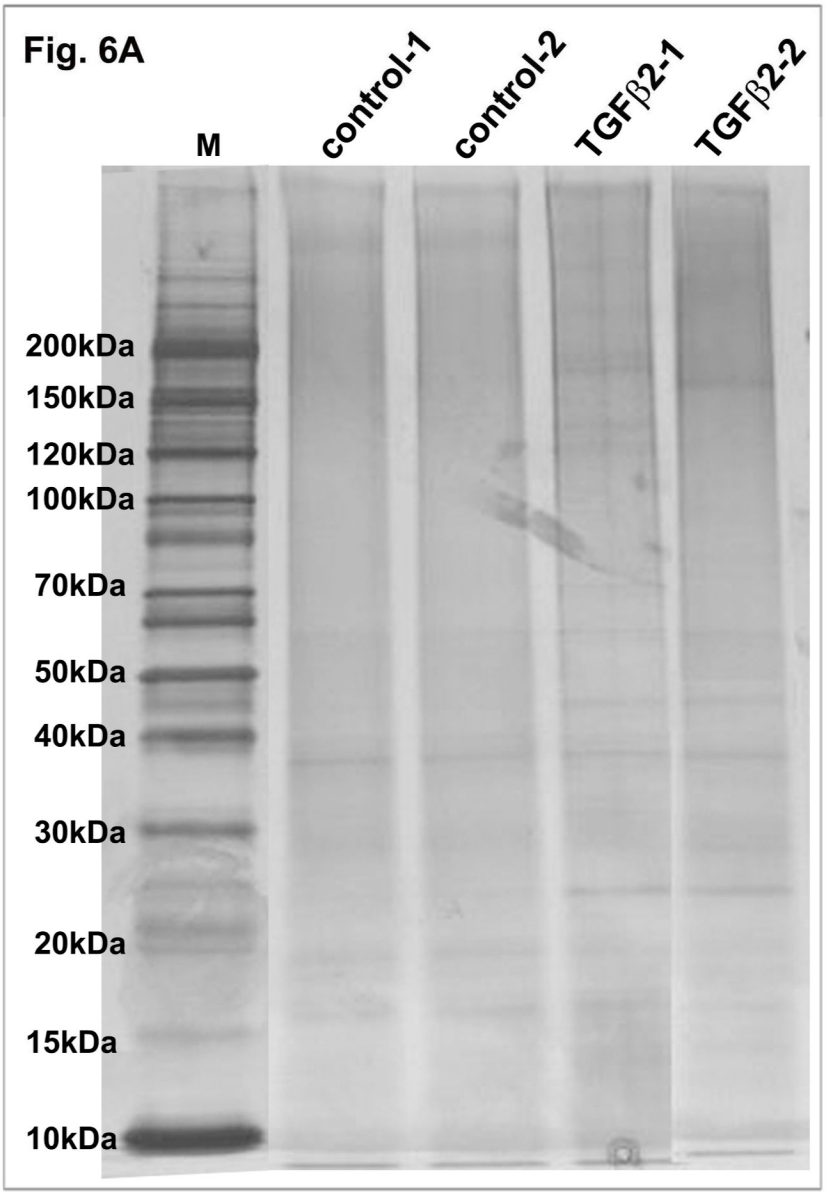

Fig. 6B

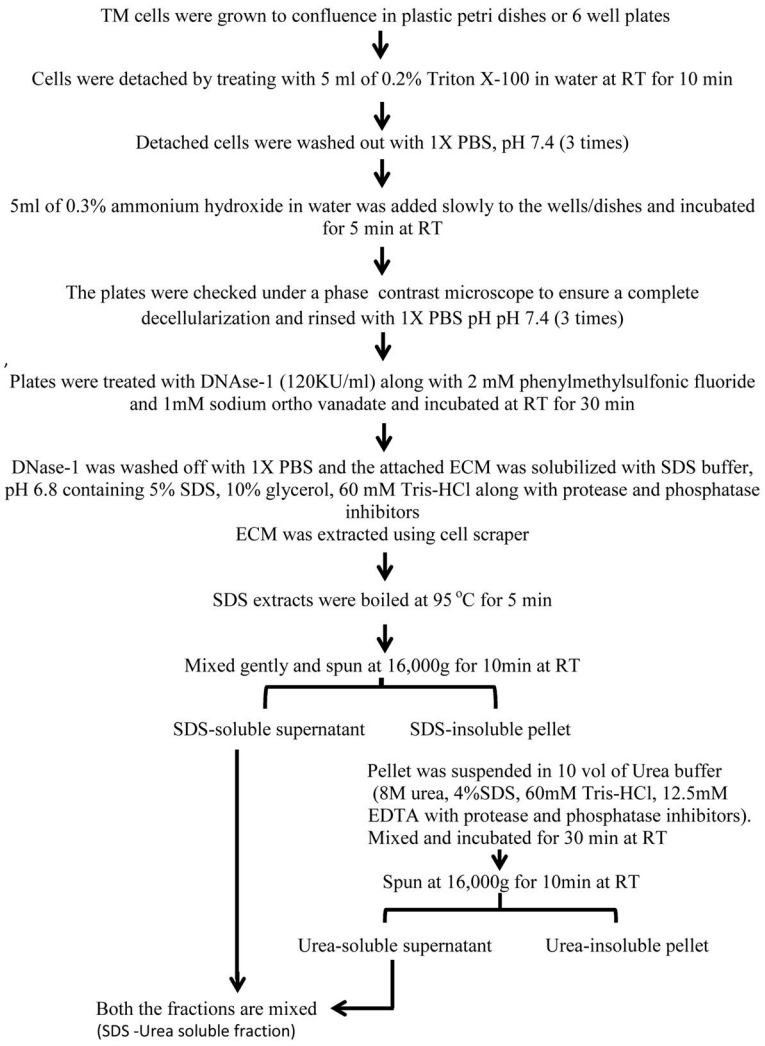

Figure 6.

TGF-β2 induced ECM accumulation in human TM cells and a schematic illustration of ECM extraction protocol. A. Serum starved human TM cells (two independent samples) treated with TGF-β2 (4 ng/ml) for 96 h showed increased production and accumulation of ECM-enriched proteins as detected by silver staining of the ECM-enriched fraction separated on a gradient SDS-polyacrylamide gel in comparison with controls cells. B. A schematic flow chart of the extraction procedure used to prepare the TM cell ECM-enriched protein fractions.

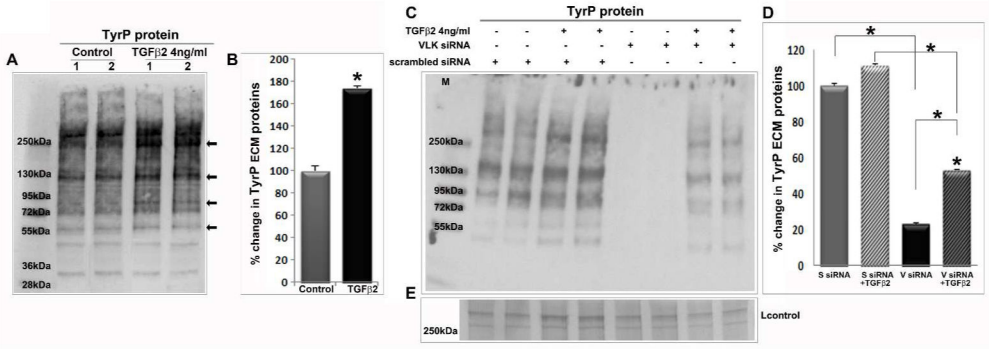

Figure 7.

Suppression of TGF-β2 induced TyrP of ECM proteins by VLK deficiency in TM cells. A. TGF-β2 induced TyrP of ECM proteins (SDS-urea soluble fraction) derived from the human TM cell cultures. Serum starved TM cells were treated with TGF-β2 (4 ng/ml) for 48 h and ECM enriched fraction was isolated as described in Fig. 6B. ECM enriched fractions were analyzed for changes in TyrP by immunoblotting and densitometric analysis. TGF-β2 treated samples (10 μg) showed a significant increase in the levels of TyrP of ECM proteins (prominent species indicated by arrows in panel A) as compared to control cells (B). Values represent the mean ±SEM of 4 independent analyses. C & D. Compared to TM cells treated with scrambled siRNA alone or together with TGF-β2, cells treated with VLK siRNA in the absence or presence of TGF-β2 showed a significant decrease in the levels of TyrP ECM proteins. Panel E shows a loading control. Values are mean ±SEM of 8 independent analyses. *P<0.05.

Table 1

Identification of ECM proteins (SDS-urea Soluble) increased by the treatment of TGF-β2 in human TM cells

UniProtKB Accession Number	ECM proteins	TGF-β2/control	Anova score (n=3)
K7EKH6	Glial fibrillary acidic protein (Fragment)	1732.97	0.006510000
P23142	Fibulin-1	15.85	0.040979342
A0A087X0S5	Collagen alpha-1(VI)chain	15.73	0.0420260000
A0A024R884	Isoform 4 of Tenascin	15.48	0.024721336
E7ESP9	Neurofilament medium polypeptide	15.12	0.040425192
Q14112	Nidogen-2	12.2	0.040200091
E9PGF5	Tensin-1	11.7	0.002057717
G3V511	Latent-transforming growth factor beta-binding protein 1	8.14	0.042187982
P51114	Fragile X mental retardation syndrome-related protein 1	7.32	0.024167427
Q8TC07	TBC1 domain family member 15	6.78	0.003585822
V9HW22	Epididymis luminal protein 113	5.53	0.000308417
A8KAJ3	EGF-containing fibulin-like extracellular matrix protein 2	4.27	0.004700989
Q05682	Caldesmon	4.12	0.000496402
P10909	Isoform 4 of Clusterin	3.88	0.047005263
Q08397	Lysyl oxidase homolog 1	3.80	0.009098022
Q69YJ3	fibulin-6 (Fragment)	3.50	0.005288116
P08493	Matrix Gla protein	3.33	0.016853000
Q15063	Periostin	3.17	0.011655584
P02545	Prelamin-A/C	2.69	0.002609079
P60709	Actin, cytoplasmic 1	2.41	0.025957847
P02751	Isoform 6 of Fibronectin	2.31	0.028456223
Q96M91	Cilia- and flagella-associated protein 53	2.28	0.009193873
Q8N6G6	ADAMTS-like protein 1	2.27	0.00991541
A8KAJ3	EGF-containing fibulin-like extracellular matrix protein 1, transcript variant 3, mRNA	2.19	0.007711977
P35580	Myosin-10	2.07	0.047654463
P11047	Laminin subunit gamma-1	2.06	0.013951701
Q9Y6C2	EMILIN-1	2.05	0.024236246
P08123	Collagen alpha-2(I) chain	1.89	0.046881349

J Cell Physiol. Author manuscript; available in PMC 2018 September 01.

UniProtKB Accession Number	ECM proteins	TGF-β2/control	Anova score (n=3)
P02452	Collagen alpha-1(I) chain	1.83	0.0386687674
A6NDY9	Filamin A	1.72	0.009971325
Q9H382	Fibronectin 1	1.69	0.007058199
P12036	Neurofilament heavy polypeptide	1.59	0.040425192

Table 2

Identification of ECM proteins (SDS-urea Insoluble) increased by the treatment of TGF-β2 in human TM cells

UniProtKB Accession Number	ECM proteins	TGF-β2/ control	Anova score (n=3)
P55001	Isoform B of Microfibrillar-associated protein 2	5420.45	0.030310641
P15502	Isoform 1 of Elastin	2383.03	0.000996696
Q08380	Galectin-3-binding protein	345.54	0.031886199
Q08397	Lysyl oxidase homolog 1	103.72	0.003609312
P08572	Collagen alpha-2(IV) chain	103.62	0.050572634
Q15582	Transforming growth factor-beta-induced protein ig-h3	89.32	0.010342166
P35556-2	Isoform 2 of Fibrillin-2	63.99	0.000896711
P28300	Protein-lysine 6-oxidase	60.64	0.056805848
P23142	Fibulin-1	54.68	0.036896707
Q9NR12	Isoform 2 of PDZ and LIM domain protein 7	38.89	0.035390200
Q05682	Caldesmon	30.07	0.010006786
P15502-	Elastin	23.97	3.24E-07
P27658	Collagen alpha-1(VIII) chain	19.52	0.001247321
O95084	Serine protease 23	18.68	0.005377157
P24821	Isoform 4 of Tenascin	17.86	0.020668783
Q6ZMP0	Thrombospondin type-1 domain-containing protein 4	17.40	0.002451091
Q15063	Periostin	16.64	0.001791472
P10909	Isoform 4 of Clusterin	16.61	0.00958499
Q8CG19	Latent-transforming growth factor beta-binding protein 1	15.81	0.008906995
P02461	Collagen alpha-1(III) chain	12.05	0.000580960
Q6S8J3	POTE ankyrin domain family member E	9.4	0.045704313
P08493	Matrix Gla protein	9.26	0.027908934
P21980	Protein-glutamine gamma-glutamyltransferase 2	9.07	0.002020116
P02452	Collagen alpha-1(I) chain	8.40	0.011448809
P08123	Collagen alpha-2(I) chain	7.46	0.008255035
P08670	Vimentin	6.06	0.011686546
P68104	Elongation factor 1-alpha 1	5.31	0.012505388
Q8WX93	Isoform 4 of Palladin	4.84	0.008290409

UniProtKB Accession Number	ECM proteins	TGF-β2/ control	Anova score (n=3)
P35556-2	Fibrillin-2	3.67	0.002732843
P60709	Actin, cytoplasmic 1	3.48	0.007046709
Q9Y6C2	EMILIN-1	3.17	0.005123759
P02751	Isoform 6 of Fibronectin	2.6	0.002583220
Q53GK6	Beta actin variant (fragment)	2.2	0.001481174
Q5SZJ2	Basement membrane-specific heparan sulfate proteoglycan core protein (Fragment)	2.0	2.07E-05
A8K9I5	Beta-1,3-glucuronyltransferase 3	2.0	0.000945761